Journal of Hepatocellular Carcinoma

Dovepress
Taylor & Francis Group

Open Access Full Text Article

ORIGINAL RESEARCH

Can Peritumoral Radiomics Based on MRI Predict the Microvascular Invasion Status of Combined Hepatocellular Carcinoma and Cholangiocarcinoma Before Surgery?

Le Guo[1,2,*], Chantao Huang[2,*], Peng Hao[2,*], Ningyang Jia[3], Ling Zhang[2,4]

[1]Lab of Molecular Imaging and Medical Intelligence, Department of Radiology, Longgang Central Hospital of Shenzhen (Shenzhen Clinical Medical College, Guangzhou University of Chinese Medicine), Shenzhen, 518116, People's Republic of China; [2]Department of Imaging Diagnosis, Nanfang Hospital, Southern Medical University, Guangzhou, 510515, People's Republic of China; [3]Department of Radiology, Shanghai Eastern Hepatobiliary Surgery Hospital, Second Military Medical University, Shanghai, 200438, People's Republic of China; [4]Medical Imaging Department of Ganzhou People's Hospital, Ganzhou, 341000, People's Republic of China

*These authors contributed equally to this work

Correspondence: Ling Zhang, Department of Imaging Diagnosis, Nanfang Hospital, Southern Medical University, Guangzhou, 510515, People's Republic of China, Tel +86-2062786561, Email zhangling_smu@163.com; Ningyang Jia, Department of Radiology, Shanghai Eastern Hepatobiliary Surgery Hospital, Second Military Medical University, Shanghai, 200438, People's Republic of China, Tel +86-02181875211, Email jianingyang6@163.com

Objective: To investigate the role of MRI peritumoral imaging in predicting microvascular invasion (MVI) status in patients with combined hepatocellular carcinoma and cholangiocarcinoma (cHCC-CCA).

Methods: Clinical and pathological data and MRI images of 118 patients with surgically resected and pathologically confirmed cHCC-CCA were retrospectively collected. The tumor in MRI images was segmented by ITK-SNAP software in three dimensions and extended 1 centimeter(cm) towards the tumor periphery. Then, the Python open-source platform was used for radiomics analysis. Mutual information and recursive elimination methods were used to select the optimal features. Clinical models and radiomics models were constructed based on six classifiers. The model's effectiveness was comprehensively evaluated using receiver operating characteristic (ROC), area under curve (AUC), and decision curve analysis (DCA), and the model results were output using Shapley Additive exPlans (SHAP).

Results: The differences in HBeAg, capsule, target sign, and lymph node metastasis between MVI negative and positive groups were statistically significant ($p < 0.05$). Based on peritumoral, 1cm fusion model (in arterial phase) has an AUC of 0.940 (95% CI: 0.801–0.947) and 0.825 (95% CI: 0.633–0.917) in the training/testing set when identifying the MVI status of cHCC-CCA. The accuracy, sensitivity, and specificity in the testing set are 0.778, 0.800, and 0.726, respectively. The DCA shows that when the threshold is approximately 11.08%–66.47%, the net return of the fusion model is higher than that of the clinical and radiomics models under the same conditions.

Conclusion: Radiomics with a 1cm extension around the tumor can improve the performance of machine-learning models in predicting MVI labels.

Keywords: peritumoral radiomics, microvascular invasion, combined hepatocellular carcinoma and cholangiocarcinoma, Shapley additive explans

Introduction

Combined hepatocellular carcinoma and cholangiocarcinoma (cHCC-CCA) is composed of both hepatocellular carcinoma (HCC) and intrahepatic cholangiocarcinoma (ICC) components, exhibiting differentiation characteristics of both hepatocytes and cholangiocytes. It is the least common pathological type of primary liver cancer, accounting for

Received: 4 January 2025
Accepted: 28 June 2025
Published: 16 July 2025

approximately 0.4% −14.2%.[1] In 1903, Tucker first proposed the definition of cHCC-CCA.[2] Subsequently, its definition and related terminology continue to be updated.[3] There is still controversy over the origin of cHCC-CCA and abnormal differentiation of liver progenitor cells and HCC may be its origin.[1,4–6] The specific etiology associated with cHCC-CCA is not yet clear. However, cHCC-CCA has the same risk factors as HCC, including hepatitis B, hepatitis C infection, and cirrhosis.[7]

Microvascular invasion (MVI) is a poor prognostic factor for surgical resection and liver transplantation in patients with primary liver cancer.[8–11] Puncture sampling or postoperative pathology were routinely used to diagnose MVI. Due to the heterogeneity within the tumor and the possibility of sampling errors caused by preoperative biopsy, the results used for detecting MVI may be unreliable. In recent years, there have been many studies on MVI, and high levels of alpha-fetoprotein (AFP), protein induced by vitamin k absence or antagonist (PIVKA-II) of serum, arterial phase tumor edge enhancement, and low signal intensity around the liver and gallbladder phases are potential biomarkers for predicting MVI status in patients with primary liver cancer.[12–14] The combination of MRI image features and radiomics has improved the prediction efficiency of MVI to varying degrees.[15–17] The preoperative prediction of MVI may play a guiding role in planning the treatment process, such as using antiviral drugs, expanding the surgical resection range, and postoperative adjuvant therapy to reduce the risk of postoperative recurrence. Although some studies involve MVI studies of cHCC-CCA, most of the differences between MVI negative and positive groups are analyzed using clinical basic features and imaging radiomics signs,[14,18,19] without further investigating the inherent differences from the heterogeneity of the tumor itself. This study aims to explore the value of enhanced MRI radiomics features of the tumor, tumor and the 1cm surrounding the tumor (hereinafter referred to as peritumoral 1cm) in the preoperative prediction of MVI in cHCC-CCA, providing a basis for clinical treatment decision-making.

Methods

Inclusion and Exclusion Criteria

This study is retrospective, and both medical center ethics committees exempted patients from informed consent. A total of 57 MVI-positive and 61 MVI-negative cases were included. We collected information on patients who underwent surgical resection of liver masses at Nanfang Hospital of Southern Medical University and Eastern Hepatobiliary Surgery Hospital in Shanghai from May 2010 to March 2021. The inclusion criteria are as follows: 1. Pathological confirmation of compliance with cHCC-CCA after surgical resection; 2. Maximum diameter ≥1cm; 3. Perform an enhanced MRI scan within four weeks before surgery; 4. Before the MRI examination, no anti-tumor treatment was performed, such as radiotherapy, transhepatic arterial chemoembolization (TACE), etc.; 5. Complete clinical and imaging data; 6. There were no tumors elsewhere in the body. Exclusion criteria: 1. Maximum diameter <1cm; 2. The contrast agent used for MRI examination is an intracellular contrast agent; 3. The presence of venous cancer thrombi is observed on MRI images; 4. Before the MRI examination, anti-tumor treatment was performed; 5. Have a history of tumors in other parts of the body; 6. Poor image quality and unclear observation of lesions. The flowchart of the cases included in this study is shown in Figure 1. After data integration, the training and test sets were randomly divided in a 7:3 ratio.

Clinical Data and Histopathology

Collect preoperative clinical data, including gender, age, AFP, cardiovascular antigen (CEA), carbohydrate antigen 199 (CA199), HBsAg, and HBeAg, which are commonly used indicators. All surgical specimens were sampled according to the 7-point baseline sample collection plan. The diagnosis of MVI was determined by histopathological examination, and cancer cell nests were observed in the vascular lumen lined with endothelial cells under a microscope. If the number of cancer cells was above 50, MVI was considered to exist. A total of 61 MVI grades 0, 48 MVI grades 1, and 9 MVI grades 2 were included in this study. Grades 1 and 2 were collectively called MVI positive, and grade 0 was negative. The diagnosis of liver cirrhosis is also determined in histopathology.

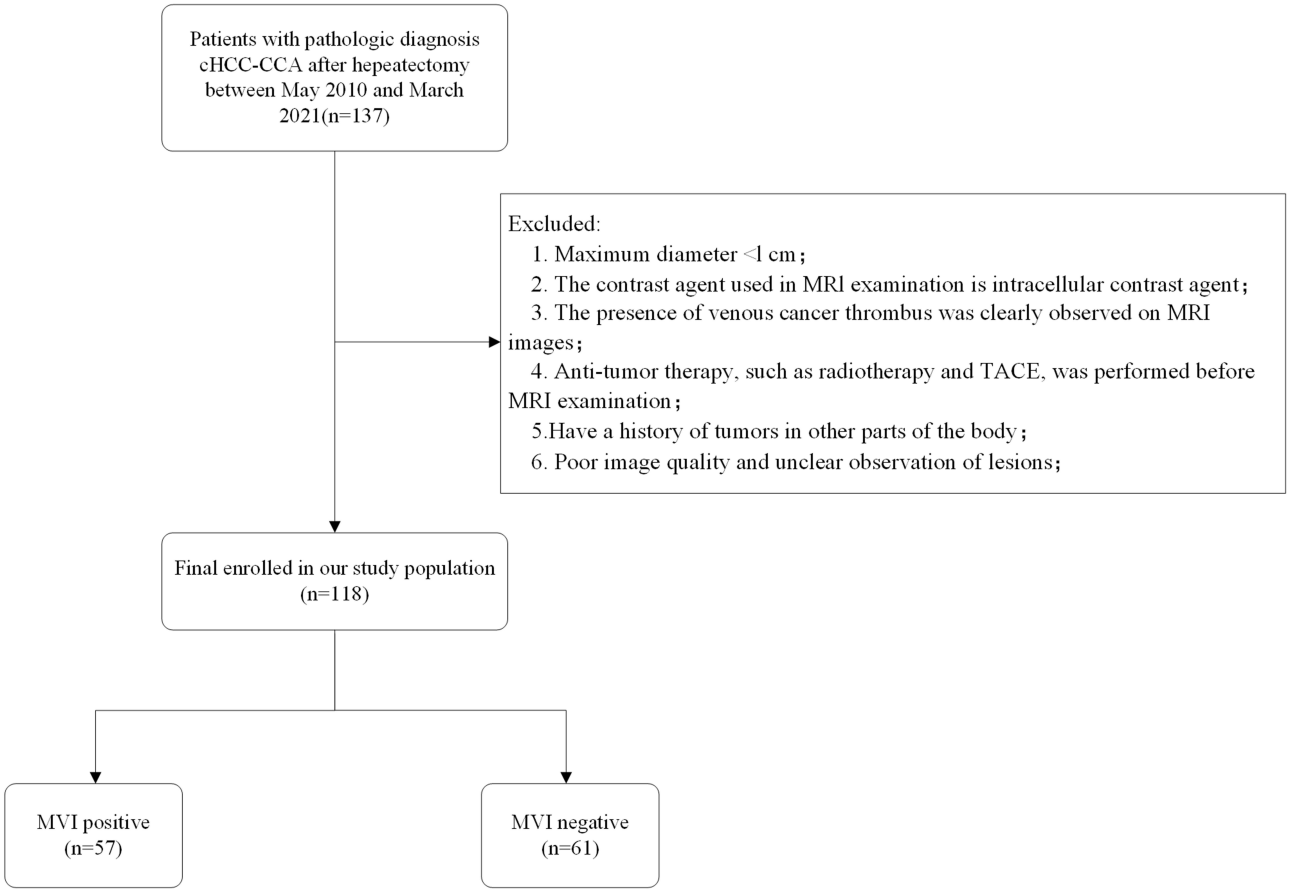

Figure 1 Data inclusion flow chart.
Abbreviations: cHCC-CCA, combined hepatocellular carcinoma and cholangiocarcinoma; TACE, transhepatic arterial chemoembolization; MVI, Microvascular invasion.

MRI Image Acquisition

The two institutions use 1.5T (General Electric, Optima MR360) and 3.0T (General Electric, Signa HDxt) scanning systems. Table 1 summarizes the scanning parameters of different machines. All patients were treated with a 16-channel abdominal coil. 0.1mmol/kg of contrast agent (Gadolinium-DTPA, Gd) was injected into the cubital vein with a high-pressure syringe at a rate of 2.0mL/s. The scanning time for each machine after the injection of the contrast agent is roughly the same. Arterial phase scanning is performed at 20–25 seconds, portal phase scanning at 50–60 seconds, and delayed phase scanning at 90–120 seconds.

Table 1 Sequences and Parameters of Dynamic-Enhanced MRI

Institution	Nanfang Hospital	Eastern Hepatobiliary Surgery Hospital
Field(T)	3.0	1.5
TR (ms) (T2/AP=PVP=DP)	3600/3.8	5100/5.0
TE (ms) (T2/AP=PVP=DP)	90/1.7	85/1.7
Angle (°) (T2/AP=PVP=DP)	90/15	90/15
ST(mm) (T2/AP=PVP=DP)	5/2.0	5/2.5
FOV	400×352	420×420
Matrix	132×114	320 × 224

Abbreviations: TR, Repetition Time; TE, Echo Time; ST, Slice Thickness; T2, T2-weighted imaging; AP, Arterial phase; PVP, Portal venous phase; DP, Delay phase; FOV, Field of View.

https://doi.org/10.2147/JHC.S515651

Image Analysis

The MRI results were evaluated by a radiologist with six years of experience in abdominal diagnosis and verified by a physician with 21 years of experience in radiological diagnosis. In case of disagreement, the two parties shall decide after discussion. They do not know the patient's clinical and pathological data. All evaluations are based on the liver imaging reporting and data system (LI-RADS) version 2018 (https://www.acr.org). The evaluation indicators include: tumor size (longest diameter on the largest cross-section, select the lesion with the longest diameter for multiple lesions), edge (whether smooth), shape (circular, elliptical, lobulated, irregular), number (number of lesions synchronously enhanced with the primary lesion), capsule, arterial phase edge enhancement (circular enhancement of arterial phase tumor edge), peritumoral enhancement during the arterial phase (crescent or polygonal enhancement area around the early arterial tumor), hepatic lobe atrophy, hepatic capsule retraction (tumor adjacent to the hepatic capsule being pulled to form an umbilical concave sign), peripheral bile duct dilation (dilation of the surrounding or distal bile duct), lipid (High signals in the in-phase are reduced in the out-phase), Target sign (low central signal, high peripheral signal on diffusion-weighted imaging), lymph node metastasis (presence of enlarged lymph nodes in the hepatic hilum and retroperitoneal area).

Radiomics Analysis

The process of radiomics analysis is shown in Figure 2.

Target Delineation

Two senior radiologists (8 and 12 years of experience in abdominal imaging diagnosis, respectively) delineated the lesions independently without knowing the pathological results. Using the open-source software ITK-SNAP (version 3.8.0), each tumor lesion was delineated layer by layer on T2 weighted imaging (T2WI), arterial phase (AP), portal vein phase (PVP), and delayed phase (DP) to form a three-dimensional region of interest. They completed lesion segmentation within four weeks. After completing the delineation of the target area, use cv2.dilate to uniformly expand the region of interest (ROI) to the surrounding

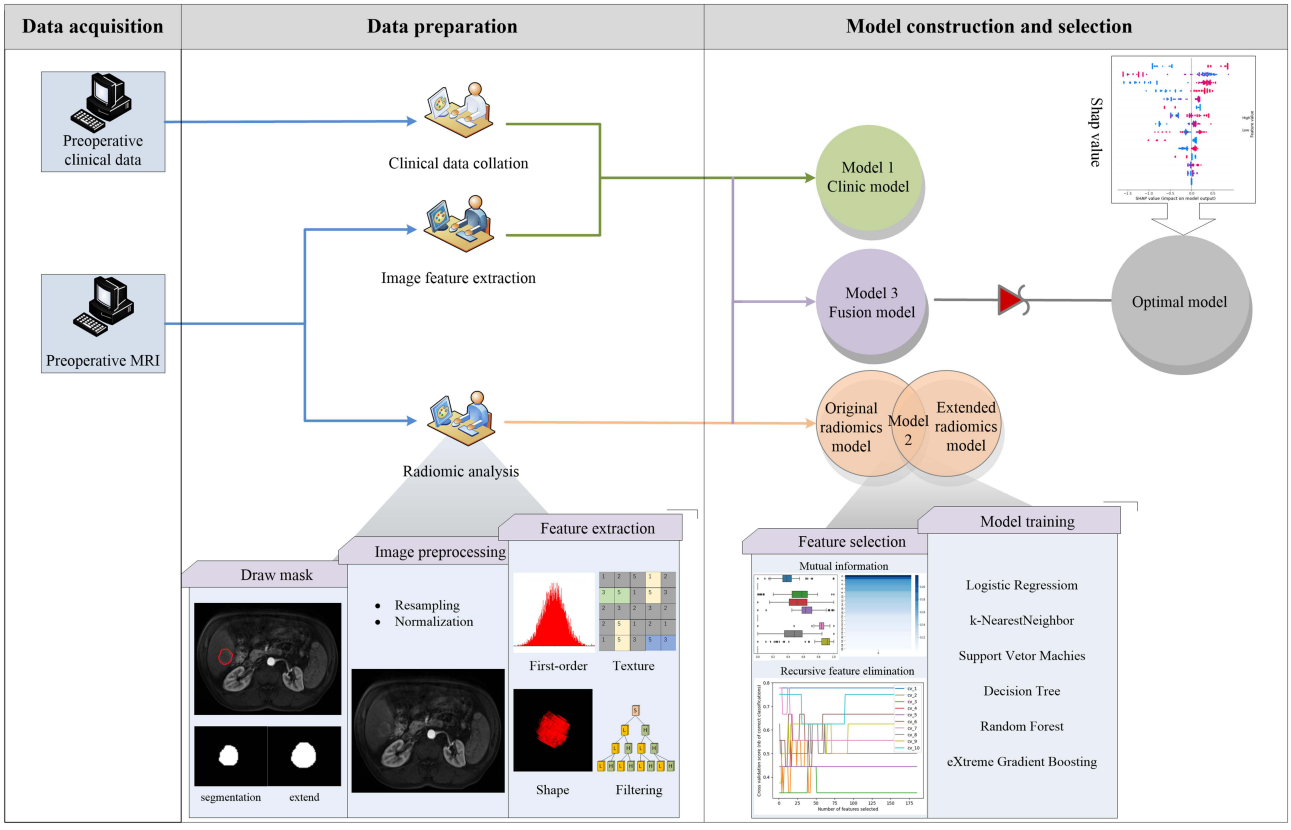

Figure 2 Radiomics flow chart.

area by 1cm, and have it verified by a doctor with eight years of experience in abdominal imaging diagnosis. Manually remove parts beyond the liver contour or covering large blood vessels such as the portal vein to avoid interfering with information and affecting model performance. Use sitkLinear and sitkNearestNeighbor to resample the original image and mask, respectively. Normalize the pixel values of the original image to 0–1 using the min-max normalization method.

Extraction and Screening of Radiomics Features

Based on the Digital Imaging and Communications in Medicine (DICOM) images and ROI of four different stages of tumors and peritumoral 1cm, initial features and peritumoral 1cm features were extracted for each region of interest using Python 3.9.7 (Pyradiomics version 2.12). To determine inter-observer consistency, we calculated the Intra-class Correlation Coefficient (ICC) for the lesions segmented by the two physicians. Those with values greater than 0.8 were included in subsequent studies, and then the feature values were normalized using the min-max method. Feature selection uses mutual information (MI) and recursive elimination (RE) method in sequence and conducts ten fold cross-validation to select the optimal feature.

Model Construction and Evaluation

Construct a clinical model based on the included clinical indicators and imaging features. The original radiomics model was constructed, respectively, based on the tumor range, and the peritumoral model was constructed within the range of peritumoral 1cm, respectively. Then, the radiomics features and peritumoral radiomics features were combined with clinical imaging features to construct fusion models and peritumoral fusion models, respectively. This study used logistic regression (LR), k-NearestNeighbor (KNN), support vector machine (SVM), decision tree (DT), random forest (RF), and eXtreme Gradient Boosting (XGB) to build different models. The models were validated using independent validation sets, and the effectiveness of the models was evaluated based on area under the curve (AUC), specificity, sensitivity, and decision curve analysis (DCA). And analyze the classification process of the model using the SHAP interpretability method.

Statistical Analysis

All statistical analyses were conducted using SPSS software (version 25.0), and a p-value <0.05 for the bilateral test statistic was considered statistically significant. Continuous variables with normal distribution are represented as mean ± standard deviation and compared with two groups using an independent sample t-test. The number of cases and percentage represent the categorical variables, and the $\chi 2$ test was used for statistical description. Bootstrapping is used to calculate the confidence interval (CI) of the AUC.

Result

Clinical Imaging Feature Analysis

The clinical baseline data and imaging analysis of cHCC-CCA patients showed a statistically significant difference ($p < 0.05$) in HBeAg, capsule, target sign, and lymph node metastasis between MVI negative and MVI positive groups. Compared with MVI-positive patients, negative patients had a higher probability of negative HBeAg. The incidence of capsule and target signs in MVI-positive patients is lower than in negative patients, but their lymph node metastasis rate is relatively high. There was no statistically significant difference in gender, age, size, number, AFP, CEA, CA199, cirrhosis, HBsAg, edge enhancement in arterial phase, peritumoral enhancement, edge, morphology, lipid deposition, hepatic lobe atrophy, capsule depression, and bile duct dilation between the two groups of cases ($p > 0.05$). The analysis of clinical and imaging characteristics of MVI positive and negative groups is presented in Table 2 and Table 3, respectively.

Imaging Radiomics Analysis

We used six different machine learning models to construct clinical, radiomics, and fusion models based on tumors and peritumoral 1cm. Table 4 lists the model performance with certain advantages among different modeling methods based on the tumor and peritumoral 1cm. The results showed that AP_SVM fusion model based on peritumoral 1cm showed the best performance in identifying the MVI status of cHCC-CCA, with AUC of 0.940 (95% CI: 0.801–0.947) and 0.825 (95% CI: 0.633–0.917) in the training/testing set, and accuracy, sensitivity, and specificity of 0.778 (95% CI: 0.639–0.889), 0.800 (95% CI: 0.563–1.000), and 0.726 (95% CI: 0.565–0.941) in the testing set, respectively. In the radiomics model, the AUC of the best

Table 2 Clinical Baseline Data Analysis of MVI Negative and Positive in cHCC-CCA

	MVI-0	MVI-1	Chi/t	*p*
Sex			0.170	0.680
Male	51(83.6%)	46(80.7%)		
Female	10(16.4%)	11(19.3%)		
Age[a]	52.44±11.367	53.51±10.245	−0.534	0.594
AFP			0.246	0.884
0-20 (μg/L)	27(44.3%)	23(40.4%)		
21-400 (μg/L)	20(32.8%)	21(36.8%)		
>400 (μg/L)	14(23.0%)	13(22.8%)		
CEA			0.683	0.409
0-5 (ng/mL)	43(70.5%)	44(77.2%)		
>5 (ng/mL)	18(29.5%)	13(22.8%)		
CA199			1.577	0.209
0-35 (u/mL)	47(77.0%)	38(66.7%)		
>35 (u/mL)	14(23.0%)	19(33.3%)		
Cirrhosis			0.150	0.698
Negative	30(49.2%)	26(45.6%)		
Positive	31(50.8%)	31(54.4%)		
HBeAg			4.753	0.029*
Negative	42(68.9%)	28(49.1%)		
Positive	19(31.1%)	29(50.9%)		
HBsAg			1.565	0.211
Negative	23(37.7%)	28(49.1%)		
Positive	38(62.3%)	29(50.9%)		

Notes: [a]Data was compared using an independent sample *t*-test. Excepted where indicated, data were compared using the χ^2 test. *p-value less than 0.05.

Abbreviations: MVI, microvascular invasion; cHCC, combined hepatocellular carcinoma and cholangiocarcinoma; AFP, alpha-fetoprotein; CEA, *carcinoembryonic antigen*; CA199, cancer antigens 199; HBeAg, hepatitis b envelope antigen; HBsAg, hepatitis b surface antigen.

Table 3 Analysis of MRI Features of MVI Negative and Positive in cHCC-CCA

	MVI-0	MVI-1	Chi	*p*
Size			0.214	0.644
≤5cm	41(67.2%)	36(63.2%)		
>5cm	20(32.8%)	21(36.8%)		
Number			1.148	0.284
Single	49(80.3%)	41(71.9%)		
Multiple	12(19.7%)	16(28.1%)		
Capsule			10.505	0.001*
Negative	27(44.3%)	42(73.7%)		
Positive	34(55.7%)	15(26.3%)		
Rim Enhancement			0.728	0.394
Negative	20(32.8%)	23(40.4%)		
Positive	41 (67.2%)	34(59.6%)		
Peritumoral Enhancement			0.161	0.688
Negative	32(52.5%)	32(56.1%)		
Positive	31(47.5%)	25(43.9%)		
Margin			0.672	0.412
Negative	27(44.3%)	21(36.8%)		
Positive	34(55.7%)	36(63.2%)		

(*Continued*)

Table 3 (Continued).

	MVI-0	MVI-1	Chi	*p*
Shape			0.988	0.804
Rotundity	12(19.7%)	9(15.8%)		
Oval	13(21.3%)	13(22.8%)		
Lobulated	21(34.4%)	17(29.8%)		
Irregular	15(24.6%)	18(31.6%)		
Lipid			1.395	0.238
Negative	54(88.5%)	46(80.7%)		
Positive	7(11.5%)	11(19.3%)		
Hepatic Lobe Atrophy			1.882	0.170
Negative	32(52.5%)	37(64.9%)		
Positive	29(47.5%)	20(35.1%)		
Capsule Depression			1.751	0.186
Negative	38(80.0%)	42(73.3%)		
Positive	23(37.7%)	15(26.3%)		
Target Sign			16.380	<0.001*
Negative	19(31.1%)	39(68.4%)		
Positive	42(68.9%)	18(31.6%)		
Bile Duct Dilation			0.401	0.526
Negative	56(91.8%)	54(94.7%)		
Positive	5(8.2%)	3(5.3%)		
Lymph Node Metastases			4.311	0.038*
Negative	57(93.4%)	46(80.7%)		
Positive	4(6.6%)	11(19.3%)		

Notes: Data were compared using the χ^2 test. *p-value less than 0.05.
Abbreviations: MVI, microvascular invasion; cHCC-CCA, combined hepatocellular carcinoma and cholangiocarcinoma.

Table 4 Comparison of Best Model Performance for Different Combinations Within Tumors and Peritumoral 1cm

Model		Accuracy (95% CI)	Precision (95% CI)	Recall (95% CI)	AUC_Test (95% CI)	AUC_Train (95% CI)	Sensitivity (95% CI)	Specificity (95% CI)
Fusion	**Expand (AP_SVM)**	0.778 (0.639–0.889)	0.706 (0.467–0.917)	0.800 (0.600–1.000)	0.825 (0.633–0.917)	0.940 (0.801–0.947)	0.800 (0.563–1.000)	0.762 (0.565–0.941)
	Original (PVP_SVM)	0.778 (0.639–0.917)	0.733 (0.500–0.947)	0.733 (0.500–0.938)	0.740 (0.617–0.906)	0.935 (0.722–0.896)	0.733 (0.500–0.944)	0.810 (0.636–0.956)
Radiomics	**Expand (AP_RF)**	0.639 (0.444–0.778)	0.542 (0.300–0.722)	0.867 (0.571–1.000)	0.775 (0.502–0.788)	1.000 (1.000–1.000)	0.867 (0.583–1.000)	0.476 (0.278–0.684)
	Original (AP_LR)	0.667 (0.500–0.806)	0.565 (0.350–0.778)	0.867 (0.688–1.000)	0.800 (0.571–0.830)	0.832 (0.612–0.827)	0.867 (0.667–1.000)	0.524 (0.300–0.793)
Clinical	**XGB**	0.611 (0.444–0.750)	0.545 (0.222–0.875)	0.400 (0.143–0.667)	0.686 (0.425–0.747)	0.890 (0.727–0.911)	0.400 (0.167–0.667)	0.762 (0.565–0.947)

Notes: Excepted where indicated, data are test set results.
Abbreviations: T2, T2-weighted imaging; AP, Arterial phase; PVP, Portal vein phase; DP, Delayed phase; AUC, area under the curve; SVM, Support vector machine; RF, random forest; LR, logistic regression.

model (Based on the tumor in the arterial phase) is 0.832 (95% CI: 0.612–0.827)/0.800 (95% CI: 0.571–0.830) (training set/test set), and the accuracy, sensitivity, and specificity in the test set are 0.667 (95% CI: 0.500–0.806), 0.867 (95% CI: 0.667–1.000), and 0.524 (95% CI: 0.300–0.739), respectively. The clinical model performed best in XGB with an AUC of 0.890 (95% CI: 0.727–0.911)/0.668 (95% CI: 0.425–0.747) (training set/test set), with accuracy, sensitivity, and specificity of 0.611 (95% CI:

0.444–0.750), 0.400 (95% CI: 0.167–0.667), and 0.762 (95% CI: 0.565–0.947) in the test set. Supplement 1–5 lists the model results of different classifiers based on tumor, peritumoral 1cm, respectively.

The optimal model DCA curve based on different modeling methods within the tumor shows that when the threshold is approximately 41.40%–52.16%, the net profit of the fusion model is higher than that of the clinical and radiomics models. Based on the DCA curves of various models with a tumor circumference of 1cm, when the threshold is approximately 11.08%–66.47%, the net profit of the fusion model is higher than that of the clinical and radiomics models. Figures 3 and 4 show the comparison of ROC curves and DCA of the optimal models in different ranges, respectively. The confusion matrix results show that in the identification of MVI status within the tumor, peritumoral 1cm, and clinically optimal models, the optimal model based on peritumoral 1cm correctly judged 16 and 12 cases of MVI negative and positive in the test set data, while the correct judgments based on the optimal models within the tumor and clinically optimal models were 11/13 and 16/6, respectively (as shown in Figure 5).

The SHAP interpreter outputs the importance of each feature in the optimal model (SVM fusion model based on peritumoral 1cm in arterial phase), ranking the top five features in sequence as capsule, target sign, capsule retraction, lipid, and arterial edge enhancement. In Figure 6, red on the right side of the y-axis indicates a positive correlation between this feature and MVI status, while red on the left indicates a negative correlation, and blue is the opposite.

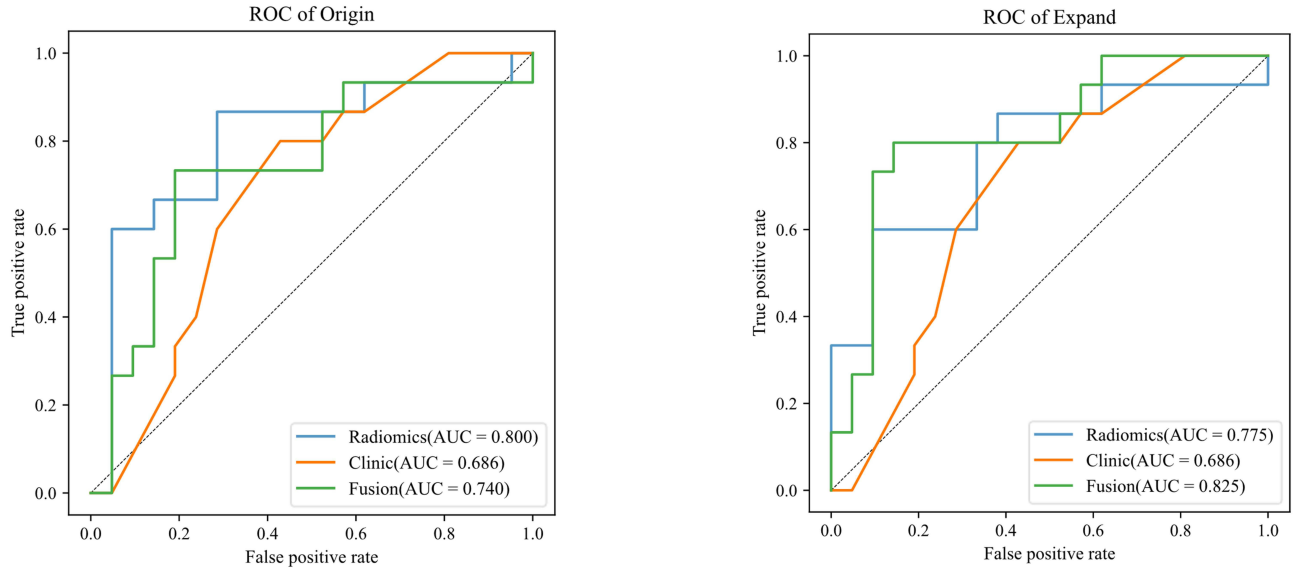

Figure 3 ROC comparison of the optimal model based on the tumor (left) and peritumoral 1cm (right).
Abbreviations: ROC, Receiver Operating Characteristic Curve; AUC, Area Under Curve.

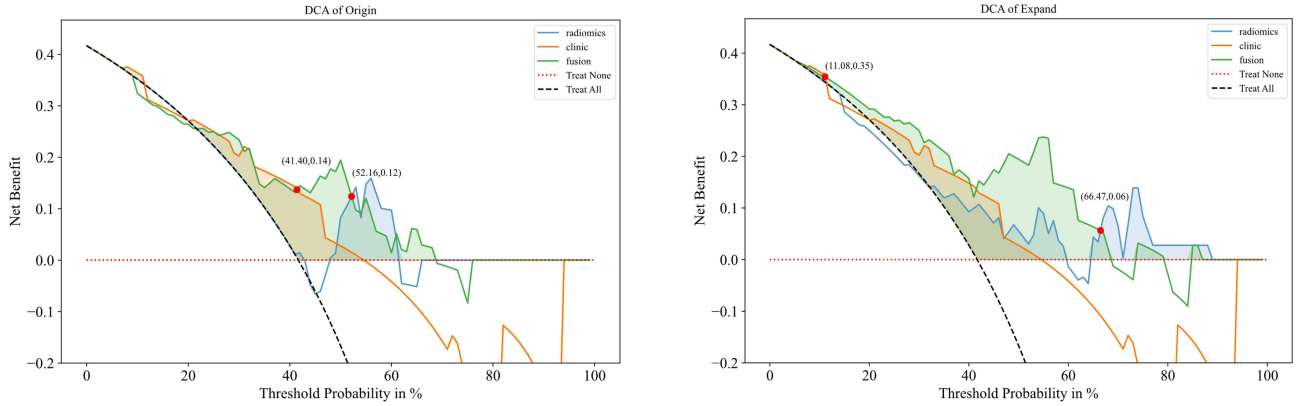

Figure 4 DCA comparison of the optimal model based on the tumor (left) and peritumoral 1cm (right).
Abbreviation: DCA, Decision curve analysis.

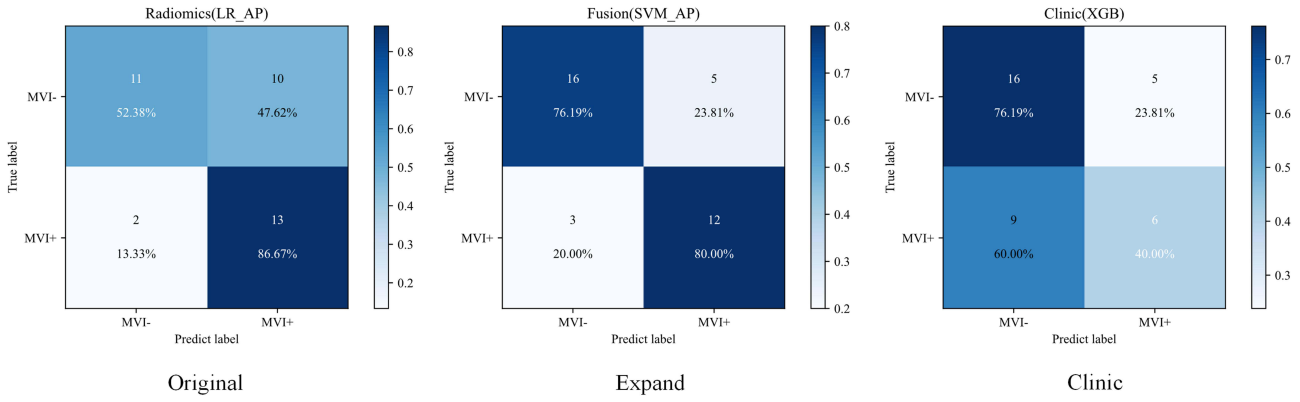

Figure 5 Optimal model confusion matrix for different combinations (tumor, peritumoral 1cm, clinical).
Abbreviations: LR, logistic regression; AP, arterial phase; SVM, support vector machine; XGB, eXtreme Gradient Boosting; MVI, Microvascular invasion.

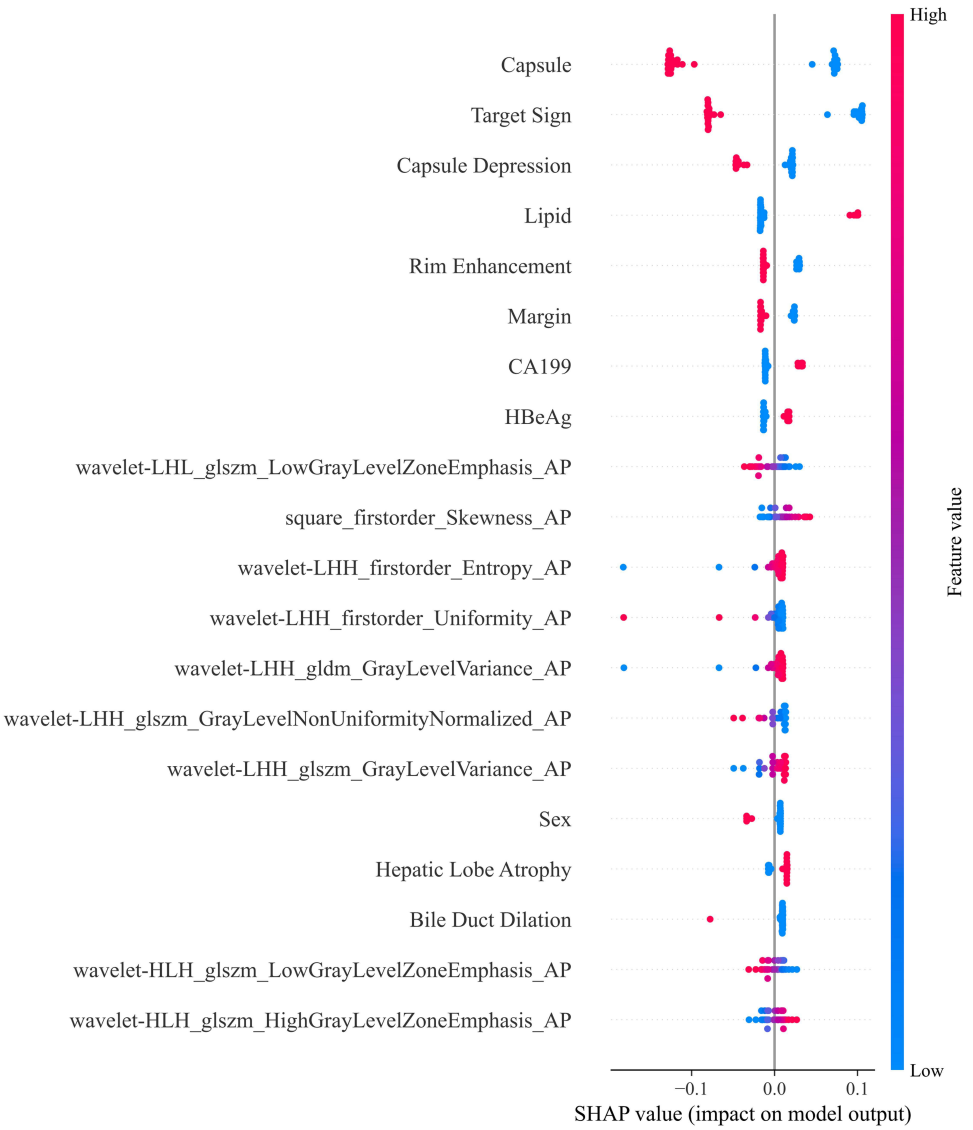

Figure 6 Shap diagram of a fusion model combined arterial phase radiomics features of peritumoral 1cm and clinical data (based on SVM). A red dot indicates that the value is positively correlated with the MVI state, while blue is the opposite.
Abbreviation: SVM: support vector machine.

https://doi.org/10.2147/JHC.S515651

Discussion

MVI, a well-established poor prognostic factor in primary liver cancer, correlates strongly with early recurrence and lower survival rates.[11] Prior studies have identified potential MVI biomarkers in cHCC-CCA, including elevated AFP, intratumoral fat deposition, and irregular arterial-phase enhancement.[13,14,20,21] However, this study contradicts these findings by demonstrating no association between AFP and MVI presence in cHCC-CCA. This discrepancy may arise from methodological limitations, including multicenter retrospective data bias, uneven distribution of MVI grades (with only a small subset of grade 2 cases), and lack of subclassification based on MVI severity. An intriguing observation in this study is the higher prevalence of HBeAg negativity among MVI-negative cHCC-CCA patients. Given the dual histological components of cHCC-CCA, prior research highlights the impact of tumor component proportions on imaging phenotypes and prognosis.[22–24] Specifically, MVI incidence increases in cHCC-CCA subgroups with >70% hepatocellular components.[24] As HBeAg is a pathological marker strongly linked to hepatocellular differentiation,[25] it may indirectly reflect tumor composition.

Recent advances in radiomics have enabled more sophisticated peritumoral tissue analysis. While most studies focus on MVI prediction in HCC,[16,26] few have explored this approach in cHCC-CCA, where clinical/imaging data remain the primary diagnostic modality.[14,18,27] This study integrates peritumoral 1cm radiomics features with clinical parameters to improve MVI detection. Consistent with prior reports,[27–29] radiomics analysis uncovered subtle textural changes in adjacent tissues undetectable by visual inspection, confirming the value of this approach.

The peritumoral 1cm range was chosen to balance practicality and diagnostic yield. Expanding beyond this threshold risks incorporating liver capsule artifacts or irrelevant tissues, while narrower margins may insufficiently capture microenvironmental heterogeneity. This decision aligns with surgical guidelines advocating <1cm resection margins combined with adjuvant radiotherapy for HCC.[30,31] However, the rarity of cHCC-CCA and lack of standardized subtyping limit the generalizability of these findings.

The influence of each feature in the optimal model on the predicted output is calculated by SHAP. The features with greater weight are all image features. Capsule, capsule retraction, lipid deposition, and tumor edge enhancement have been identified as potential signs associated with MVI status in patients with primary liver cancer.[12,13,15] However, Huang et al believed there was no difference between tumor edge enhancement and lipids in the MVI status of cHCC-CCA patients.[19] The target signs indicated that there were cystic and necrotic areas in the center of the tumor, and the signal attenuation on DWI might be due to the in vasive growth of the tumor, the rapid growth of the tumor leading to internal blood supply insufficiency, local infection and other reasons, which reflected MVI to some extent. These findings reinforce the complementary roles of radiomics and serum biomarkers in clinical diagnostics.[15] It was found that there were incorrect MVI classifications in the model. Among the three false negative cases, HBsAg, cirrhosis and rim enhancement were all positive, while capsule depression was all negative. This is quite different from the five false positive cases. We found that some of the results did not conform to the SHAP analysis results. It might be caused by the selection bias resulting from the small sample size or by the underfitting effect in the model training process. In the future, efforts need to be made to overcome adverse outcomes from these aspects.

Clinical utility analysis demonstrated superior net benefit for the fusion model compared to standalone clinical/radiomics models. The peritumoral 1cm based model exhibited a wider risk threshold range, enabling more balanced decision-making between therapeutic benefits and risks.[32,33]

Our research has several limitations. Firstly, due to the data from multiple centers and the uneven sample size among different centers, a single central data was not used as the training, testing, and external validation sets. Secondly, our study did not classify cHCC-CCA into different subtypes based on its latest classification, exploring the differences in MVI among different subtypes and differential diagnosis, which also needs further research in the future. Finally, the subjects included in this study were all patients who underwent surgical resection, and some patients may have received empirical anti-HCC treatment without undergoing pathological examination, which led to some selection bias.

Conclusion

Our research indicates that using machine learning algorithms for comprehensive analysis of imaging radiomics features within peritumoral 1cm can more accurately predict the MVI status of cHCC-CCA patients and explain the evaluation process of the model in decision-making through the SHAP method.

Abbreviations

MVI, microvascular invasion; cHCC, combined hepatocellular carcinoma and cholangiocarcinoma; cm, centimeter; ROC, receiver operating characteristic; AUC, area under curve; DCA, decision curve analysis; SHAP, Shapley Additive exPlans; HCC, hepatocellular carcinoma; ICC, intrahepatic cholangiocarcinoma; AFP, alpha-fetoprotein; PIVKA-II, protein induced by vitamin k absence or antagonist II; CEA, carcinoembryonic antigen; CA199, cancer antigens 199; HBeAg, hepatitis b envelope antigen; HBsAg, hepatitis b surface antigen; LI-RADS, liver imaging reporting and data system; T2WI, T2 weighted imaging; AP, arterial phase; PVP, portal vein phase; DP, delayed phase; LR, logistic regression; KNN, k-NearestNeighbor; SVM, support vector machine; DT, decision tree; RF, random forest; XGB, eXtreme Gradient Boosting; CI, confidence interval.

Data Statement

We confirm that all clinical data contained in this study have been anonymous or confidential.

Ethical Approval and Consent to Participate

The study were approved by the Southern Medical University Nangfang Hospital Ethics Review Committee and Shanghai Eastern Hepatobiliary Surgery Hospital Ethics Review Committee, and written informed consent was not required for this study because MRI has been used clinically as a standard imaging examination.

Consent to Publish

This publication has been approved by the responsible authorities at the institution where the work is carried out.

Acknowledgments

We want to thank the whole study team at 4 Hospitals for their continuous support. In addition, we would like to express our gratitude to Zhongjian Liao for the data support provided for this research.

Funding

This study has received funding from the Natural science foundation of Guangdong province (2018A030313951), the Science and Technology Plan Project of Ganzhou (2022–RC1339, 2023LNS17497), and the Medical Scientific Research Foundation of Guangdong Province, China (No.B2025403).

Disclosure

The author(s) reports no conflicts of interest in this work.

References

1. Beaufrère A, Calderaro J, Paradis V. Combined hepatocellular-cholangiocarcinoma: an update. *J Hepatol*. 2021;74(5):1212–1224. doi:10.1016/j.jhep.2021.01.035
2. EFG I M S T. Primary cancer of the liver. *Ind Med Gaz*. 1903.
3. Allen RA, Lisa JR. combined liver cell and bile duct carcinoma. *Am J Pathol*. 1949;4:647–655.
4. Wang G, Wang Q, Liang N, et al. Oncogenic driver genes and tumor microenvironment determine the type of liver cancer. *Cell Death Dis*. 2020;11.
5. Rosenberg N, Van Haele M, Lanton T, et al. Combined hepatocellular-cholangiocarcinoma derives from liver progenitor cells and depends on senescence and IL-6 trans-signaling. *J Hepatol*. 2022;77(6):1631–1641. doi:10.1016/j.jhep.2022.07.029
6. Schizas D, Mastoraki A, Routsi E, et al. Combined hepatocellular-cholangiocarcinoma: an update on epidemiology, classification, diagnosis and management. *Hepatobiliary Pancreatic Dis Int*. 2020;19(6):515–523. doi:10.1016/j.hbpd.2020.07.004
7. Liu C, Fan S, Lo C, et al. Hepatic resection for combined hepatocellular and cholangiocarcinoma. *Archiv Surg*. 2003;138(1):86–90. doi:10.1001/archsurg.138.1.86
8. Wang T, Yang X, Tang H, et al. Integrated nomograms to predict overall survival and recurrence-free survival in patients with combined hepatocellular cholangiocarcinoma (cHCC) after liver resection. *Aging*. 2020;12(15):15334–15358. doi:10.18632/aging.103577
9. Tang Y, Wang L, Teng F, Zhang T, Zhao Y, Chen Z. The clinical characteristics and prognostic factors of combined hepatocellular carcinoma and cholangiocarcinoma, hepatocellular carcinoma and intrahepatic cholangiocarcinoma after surgical resection: a propensity score matching analysis. *Int J Med Sci*. 2021;18(1):187–198. doi:10.7150/ijms.50883
10. Wang Y, Zhou C, Zhu G, et al. A multidimensional nomogram combining imaging features and clinical factors to predict the invasiveness and metastasis of combined hepatocellular cholangiocarcinoma. *Ann Translat Med*. 2021;9(20):1518. doi:10.21037/atm-21-2500

11. Wu Y, Liu H, Zeng J, et al. Development and validation of nomogram to predict very early recurrence of combined hepatocellular-cholangiocarcinoma after hepatic resection: a multi-institutional study. *World J Surg Oncol*. 2022;20(1):20. doi:10.1186/s12957-022-02488-3
12. Zhang L, Yu X, Wei W, et al. Prediction of HCC microvascular invasion with gadobenate-enhanced MRI: correlation with pathology. *Eur Radiol*. 2020;30(10):5327–5336. doi:10.1007/s00330-020-06895-6
13. Wang X, Wang W, Ma X, et al. Combined hepatocellular-cholangiocarcinoma: which preoperative clinical data and conventional MRI characteristics have value for the prediction of microvascular invasion and clinical significance? *Eur Radiol*. 2020;30(10):5337–5347. doi:10.1007/s00330-020-06861-2
14. Zhang J, Dong W, Li Y, Fu J, Jia N. Prediction of microvascular invasion in combined hepatocellular-cholangiocarcinoma based on preoperative contrast-enhanced CT and clinical data. *Eur J Radiol*. 2023;163:110839. doi:10.1016/j.ejrad.2023.110839
15. Yang W, Zhu F, Chen W. Texture analysis of contrast-enhanced magnetic resonance imaging predicts microvascular invasion in hepatocellular carcinoma. *Eur J Radiol*. 2022;156:110528. doi:10.1016/j.ejrad.2022.110528
16. Qu C, Wang Q, Li C, et al. A radiomics model based on Gd-EOB-DTPA-enhanced MRI for the prediction of microvascular invasion in solitary hepatocellular carcinoma ≤ 5 cm. *Front Oncol*. 2022;12.
17. Lv K, Cao X, Du P, Fu JY, Geng DY, Zhang J. Radiomics for the detection of microvascular invasion in hepatocellular carcinoma. *World J Gastroenterol*. 2022;28(20):2176–2183. doi:10.3748/wjg.v28.i20.2176
18. Liao Z, Lu L, Liu Y, et al. Clinical and DCE-CT signs in predicting microvascular invasion in cHCC-ICC. *Cancer Imaging*. 2023;23(1):23. doi:10.1186/s40644-023-00538-x
19. Huang S, Zuo M, Xie C. Combining preoperative clinical and imaging characteristics to predict MVI in hepatitis B virus-related combined hepatocellular carcinoma and cholangiocarcinoma. *J Personal Med*. 2023;13(2):246. doi:10.3390/jpm13020246
20. Hou GM, Jiang C, Du JP, Yuan KF. Sarcopenia predicts an adverse prognosis in patients with combined hepatocellular carcinoma and cholangiocarcinoma after surgery. *Cancer Med*. 2022;11(2):317–331. doi:10.1002/cam4.4448
21. Chen Y, Lu Q, Zhu Y, Huang B, Dong Y, Wang W. Prediction of microvascular invasion in combined hepatocellular-cholangiocarcinoma based on preoperative clinical data and contrast-enhanced ultrasound characteristics. *Ultrasound Med Biol*. 2022;48(7):1190–1201. doi:10.1016/j.ultrasmedbio.2022.02.014
22. Kim KH, Lee SG, Park EH, et al. Surgical treatments and prognoses of patients with combined hepatocellular carcinoma and cholangiocarcinoma. *Ann Surg Oncol*. 2009;16(3):623–629. doi:10.1245/s10434-008-0278-3
23. Sheng R, Yang C, Zhang Y, et al. The significance of the predominant component in combined hepatocellular-cholangiocarcinoma: MRI manifestation and prognostic value. *Abdom Radiol*. 2023;128:1047–1060.
24. Zhou C, Lu X, Wang Y, Qian X, Yang C, Zeng M. Histopathological components correlated with MRI features and prognosis in combined hepatocellular carcinoma-cholangiocarcinoma. *Eur Radiol*. 2022;32(10):6702–6711. doi:10.1007/s00330-022-09065-y
25. Lampertico P, Agarwal K, Berg T, et al. EASL 2017 clinical practice guidelines on the management of hepatitis B virus infection. *J Hepatol*. 2017;67(2):370–398. doi:10.1016/j.jhep.2017.03.021
26. Shan Q, Hu H, Feng S, et al. CT-based peritumoral radiomics signatures to predict early recurrence in hepatocellular carcinoma after curative tumor resection or ablation. *Cancer Imaging*. 2019;19(1):19. doi:10.1186/s40644-019-0203-y
27. Na HY, Kim JH, Kim H, et al. Multiregional analysis of combined hepatocellular-cholangiocarcinoma reveals histologic diversity and molecular clonality. *Histopathology*. 2023;84(2):402–408. doi:10.1111/his.15081
28. Chong H, Yang L, Sheng R, et al. Multi-scale and multi-parametric radiomics of gadoxetate disodium–enhanced MRI predicts microvascular invasion and outcome in patients with solitary hepatocellular carcinoma ≤ 5 cm. *Eur Radiol*. 2021;31(7):4824–4838. doi:10.1007/s00330-020-07601-2
29. Gao L, Xiong M, Chen X, et al. Multi-region radiomic analysis based on multi-sequence MRI can preoperatively predict microvascular invasion in hepatocellular carcinoma. *Front Oncol*. 2022;12.
30. Yu W, Wang W, Rong W, et al. Adjuvant radiotherapy in centrally located hepatocellular carcinomas after hepatectomy with narrow margin (<1 cm): a prospective randomized study. *J Am College Surg*. 2014;218(3):381–392. doi:10.1016/j.jamcollsurg.2013.11.030
31. Wang L, Liu Y, Rong W, et al. The role of intraoperative electron radiotherapy in centrally located hepatocellular carcinomas treated with narrow-margin (<1 cm) hepatectomy: a prospective, Phase 2 study. *Hepatobiliary Surg Nutrit*. 2022;11:515–529.
32. Vickers AJ, Cronin AM, Elkin EB, Gonen M. Extensions to decision curve analysis, a novel method for evaluating diagnostic tests, prediction models and molecular markers. *BMC Med Inform Decis Mak*. 2008;8(1):53. doi:10.1186/1472-6947-8-53
33. Vickers AJ, Elkin EB. Decision curve analysis: a novel method for evaluating prediction models. *Med Decis Mak*. 2006;26(6):565–574. doi:10.1177/0272989X06295361